X-611-65-94
NASA TM X-55245

REVIEW OF GALACTIC AND SOLAR COSMIC RAYS

BY
F. B. McDONALD

MARCH 1965

NASA
GODDARD SPACE FLIGHT CENTER
GREENBELT, MARYLAND

Goddard Energetic Particles Preprint Series

Review of Galactic and Solar Cosmic Rays

F. B. McDonald

Goddard Space Flight Center
Greenbelt, Maryland

Introduction

The energetic particle population in interplanetary space extends from "solar wind" protons in the kev range to ultra-relativistic particles associated with the galactic cosmic rays. The population in this region of space is highly variable. Not only are the galactic cosmic rays strongly modulated by the solar wind, but there are frequent great injections of solar cosmic rays that give rise to particle fluxes an order of magnitude greater than galactic cosmic rays. Interspersed with these events are small recurrent streams associated with particularly active solar regions and producing streams of protons in the 1-10 Mev range. This paper attempts to summarize some salient features of both the galactic and solar cosmic rays.

Galactic Cosmic Rays

The galactic cosmic rays were first discovered some 50 years ago, but even now their study is one of the important problems in physics and astrophysics. Following Warld War I, until the late 1940's, cosmic ray studies were nearly synonymous with high energy physics. The nuclear interactions of the high energy primaries with the nuclei of the upper atmosphere, and the resulting electron and nuclear cascades down through the atmosphere, furnished the particle beam for discovering the positively charged electron (positron), the μ and π meson, and the early heavy mesons or "strange particles". Since the cosmic rays interact

with air nuclei, it is clearly necessary to get beyond the earth's atmosphere to obtain quantitative studies of most of the properties of the primary beam. With the development of large Skyhook balloons and, more importantly, the advent of earth satellites and probes, it has been possible to obtain far more definitive information on the nature of the primary radiation. Strongly coupled with this is the discovery of great discrete radio sources emitting polarized radio signals which can apparently only be explained in terms of synchrotron radiation from highly relativistic electrons. This important link to astrophysics is further emphasized when we realize that the energy density of the primary radiation is about 1 electron volt per cubic centimeter. This is comparable to the energy density of starlight, to the energy contained in the galactic magnetic fields, and to the energy due to turbulence through the galaxy. Because of the very great energy of the particles, we assume they cannot be contained in our solar system and are therefore generated in the galaxy, possibly by a variety of sources. When we observe them near the earth's orbit they have already undergone three basic processes: (1) initial acceleration followed by diffusion through the galaxy, (2) possible post-acceleration, and finally, (3) modulation by the solar wind. However, it is more convenient to order the experimental information in the following way: (a) chemical composition or charge distribution, (b) energy distribution, (c) spatial distribution.

Charge Distribution

The multiply charged particles observed in the primary cosmic ray beam furnish us a direct sample of galactic material. Figure 1 demonstrates one method of doing high energy chemistry[1]. Illustrated here are tracks of heavy nuclei, ranging from hydrogen through iron, in a nuclear emulsion. As one progresses towards the heavier nuclei the strong coulomb interaction between the stripped nucleus and the electrons of the elements in the emulsion produces

delta rays or "knock-on" electrons, which provide one means of charge identification. The measurements to date on the chemical abundances are summarized[2,3] in Tables 1 and 2. The striking feature here is the overabundance of elements in the range greater than carbon and the presence of lithium, beryllium and boron. This suggests two things: First, that the initial injection and acceleration of cosmic rays occur in a region rich in heavy nuclei; second, that the light nuclei Li, Be, B are formed by fragmentation of these heavy nuclei in nuclear collisions with interstellar hydrogen. We know reasonably well[3] the fragmentation parameters for the production of Li, Be and B in the breakup of heavy nuclei, and this makes it possible to estimate the average amount of material traversed by the cosmic rays. The best current estimate[4] is 2.5 gms/cm^2. Table 2 shows further details of the chemical composition; it reveals that the nuclei of even Z tend to predominate over those of odd Z. There also appears to be a dearth of elements in the region just before calcium. Recent studies have indicated that electrons in the energy interval greater than 100 Mev constitute approximately 1% of the primary beam[5,6].

Energy Distribution

The next distinguishing feature of the galactic radiation is the energy spectrum. Observations now extend from 10^7 to 10^{19} electron volts. Particles with total energies of approximately 10^{20} electron volts have been observed[7]. Figure 2 shows the integral flux values over the complete range. In the region up to approximately 20 Bev data have been obtained[8,9] by direct observations with satellites, space probes, or balloons. The intermediate region around 10^{12} EV data have been obtained by the study of high energy interactions underground[10,11]; and the highest energy ($> \sim 10^{15}$ EV) data are based on studies of extensive air

showers[12,13,14]. The best estimate now is that if we represent the integral spectra in the form

$$J(\geq E) = \frac{K}{(1+E)^{\gamma}} \text{ particles/cm}^2\text{-sec-ster with kinetic energy } >E(\text{Bev})$$

γ changes from 1.5 at the lowest energy interval to a value in the range 1.7-2.17 at the highest. Recent data tend to suggest that at even higher energies γ possibly assumes a smaller value. The best experimental evidence at present indicates that in the range 10^9 to 10^{15} EV the charge composition is not a function of energy. As one goes to much lower energies, it is expected that the energy loss in the traversal of the 2.5 gms/cm^2 of hydrogen will play an important role and one should then see different energy spectra in this region for different components. Figure 3 shows the low energy differential spectra for protons extending down to approximately 10 Mev. These measurements[15-19] were taken in mid 1963 and 1964 and presumably represent conditions just prior to solar minimum. It is observed that the low energy portion of the spectrum is steeply falling as a function of energy. In the region 10-100 Mev these measurements were made aboard the IMP-1 spacecraft.

Spatial Distribution

It appears that the primary cosmic radiation is essentially isotropic over the celestial sphere. The amplitude of anisotropy[20,21] is probably not greater than 1% in the region up to approximately 10^{15} EV. At medium energies (greater than $\sim$ 500 Mev) there may be small anisotropies associated with the solar modulation. Studies in the low energy range (10 Mev to approximately 300 Mev, for example, have not been made.

Solar Cosmic Rays

During the period 1956-1963 there were at least 64 occasions when the sun accelerated nuclei to energies greater than a few Mev and these particles were subsequently detected in the vicinity of the earth. These solar cosmic ray events are of fundamental scientific importance. Not only should they provide information on solar processes, but their propagation characteristics should give new clues to the magnetic field configurations in the vicinity of the sun and in interplanetary space. These solar particle outbursts also pose important considerations for manned space travel in such programs as the forthcoming Apollo flights. Some of the pertinent features of these events - size and frequency of occurrence, energy and charge spectra, and propagation characteristics will be summarized here.

Frequency and Size Distribution

The solar production of cosmic rays was first observed by Forbush[22] in 1942 by means of sea level ionization chambers. Neutron monitors, introduced in 1949, offered greater sensitivity but still responded primarily to particles with kinetic energies >1BEV at the top of the atmosphere. The identification of polar-cap absorption events with solar particle emission by Bailey[23] provided a means of extending the observations to much lower particle energies. This method was extended by Reid and Collins[24]. It is based on the attenuation of galactic radio noise due to the enhanced ionization produced by these events in the vicinity of the polar D layer. Finally, the direct particle observations by balloon, rocket, and satellite borne instrumentation have greatly extended our knowledge of these events. By using all these methods[25] some 64 events

have been detected over the interval around solar maximum (Table 3). There were probably additional small events which were not detected.

Because of the uncertainty in the detection of small events, it seems worthwhile to introduce a threshold and consider only those events which are greater than this threshold. The arbitrarily chosen limit is those with a minimum integrated intensity of 10^6 particles/cm^2 at energies > 30 Mev observed at the earth. (This is comparable to the integrated intensity of the galactic cosmic radiation for one week.) This, then, reduces the total number of events to 30 over the six year period. The integrated intensities of these events are summarized in Table 4[24].

The November 12 and 15, 1960 events certainly are two of the largest events ever recorded. Since these two events were studied in detail by a number of rocket, balloon and satellite observations combined with numerous riometer and neutron monitor measurements, they are by far the best documented of the great events. The time history of these two events[26] is shown in Figures 4 and 5. It is to be understood that the second event follows immediately after the first. In the 12 November event there are two maxima displayed in the > 500 Mev region. The second maximum is associated with the passage of a plasma cloud that also generated a large magnetic storm and produced a Forbush decrease (which can be described as a depression or sweeping out of the galactic cosmic rays).

The event on 15 November 1960 was marked by strong anisotropy during the first hour[27]. The high intensity phase has a very rapid rise followed by a regular decay (Figure 5). The integral flux greater than 20 Mev reached a maximum 20 hours after the flare. Again in Figure 5 the integral time history

at three energy levels is shown.

Charge Composition

The charge composition of the cosmic radiation was first studied extensively by Fichtel et al[28,29]. They observed a proton/medium nuclei (Medium nuclei = carbon, nitrogen and oxygen) ratio of ~2000 in the energy range 42.5 Mev to 95 Mev; a proton/helium ratio of 33 in the same energy interval, and a helium/medium ratio of 60. While these small abundances imply that heavy nuclei are not of importance from the manned space travel viewpoint, nevertheless the fact that the sun accelerates these nuclei to moderate energies is of enormous astrophysical significance. The charge spectrum of Biswas, Fichtel and Guss is given in Table 5. All values have been normalized to a base of oxygen = 10. Also shown for comparison is the relative abundance in the solar atmosphere and in the galactic cosmic rays. It is seen that the solar cosmic rays agree well with the relative abundance in the solar atmosphere and differ significantly in several areas from that observed in the galactic cosmic rays.

Energy Spectrum of the Solar Cosmic Rays

It is important to determine the spectral characteristics of the solar cosmic rays. To date the methods it has been possible to devise cover only a small dynamic range in energy for fixed n. The general practice has been to represent the differential spectrum of the solar particles in the form $dJ/dE = K/E^n$ where E is the kinetic energy and n varies over the range 1-6. In order to apply this formula over an extended dynamic range it is necessary to vary n as a function of energy, i.e., to have n decrease as the energy decreases. The measurements of alphas and heavy nuclei strongly suggest that both charge

components display the same rigidity spectrum[28]. It is most convenient to think of rigidity simply as momentum per unit charge. Freier and Webber[30] have proposed a representation in the form of exponential rigidity as given by the formula

$$\frac{dJ}{dP} = \frac{dJ_o(t)}{dP} \exp\left[-\frac{P}{P_o(t)}\right],$$

where P_o is a characteristic rigidity which is a function of time, dJ_o/dP also is a function of time and P is the particle rigidity. This has produced a remarkable simplification of the spectra of the solar cosmic rays as shown in Figure 6. It is still debatable how low in energy a rigidity representation can be extended. In most events it is not applicable in the region below 50-30 Mev; below 30 Mev it predicts an intensity which is too low compared to the observations. It does, however, appear to be well followed in the higher energy regions. It has been observed that both P_o and J_o are functions of time. These are shown for the November 1960 events in Figure 7. The conventional representation for these events has been discussed in a previous section of this paper. While P_o appears simply to decrease as a function of time, J_o displays a complex behavior which is probably strongly dependent on the interplanetary electromagnetic conditions near the earth's orbit. For example, at the time of the November 15 cosmic ray flare a solar plasma front was enroute to the earth from a previous flare in the same solar region. Following the sudden commencement on November 15 the total intensity of solar particles increased by an order of magnitude and the spectrum steepened appropriately. This is reflected in the strong increase in J_o at that time. A similar behavior is noted for the plasma cloud associated with the 12 November event. It is important to note that this technique is not applicable for the onset or beginning of the solar flare and applies only when a reasonable equilibrium

has been established following flare maximum.

Propagation Characteristics

The data obtained from the satellites and space probes have made it possible to observe in detail the onset and decay phase for a number of solar proton events. One example of a great variety of data that has been collected by a number of observers is the 85 Mev data from Explorers XII and XIV which is shown in Figure 8. The detailed energy spectrum for the 28 September 1961 event is shown as a function of time[31,32](Figure 9). This particular event can be characterized as medium sized but contains several striking features. For example, in Figure 10 the behavior of the intensities of the various differential components for this event has been plotted not as a function of time but simply as a function of distance travelled. Distance travelled is simply the product of particle velocity and the time from the flare. The intensity curves of the various components have then been vertically scaled to give the best fit to a common curve. It is then noted that all components lie very closely on a common curve. This has been interpreted by the authors as a measure of the probability that a particle should travel a given distance before reaching the earth from the sun.

The fact that they fall on a common curve shows that particles of all energies travel a given path length with equal probabilities. The distance travelled by most particles is an order of magnitude larger than one astronomical unit. This indicates that propagation involves an important degree of scattering. Furthermore, in the energy region studied, i.e., below 1 bev, the degree of scattering is not a function of energy. This suggests that the mode of propagation is a diffusion-like process. A number of other observers[32,34] have been

able to fit solar proton data to a simple diffusion process as represented by[33]

$$\mu(M,t) = \frac{N}{2\pi^{1/2}\ \tau^{3/2}} \exp - \frac{MR}{4\tau} \quad ,$$

where N = particle/unit energy/solid angle at source measured at $\tau = 0$,

R = distance from source, and $\tau = Qt$ where $Q = w\ \lambda/3$, w= particle velocity,

λ = diffusion mean free path.

It has also generally been necessary to add a boundary to explain the observed change from a power law to exponential data. The present simple representation of velocity dependence makes it possible to extrapolate back to zero distance[31], and this extrapolation makes it possible to determine the source spectrum. These are shown for a number of events in Figure 11. The source spectra appear to be well represented by power laws in kinetic energy. This is not in disagreement with the representation of the spectra in the form of exponential rigidity. In the latter case one is dealing with particles after they have propagated through interplanetary space, while the source spectra represent the particles at the sun immediately following acceleration. In the event of 28 September 1961 a great increase was observed at the time of the large magnetic storm some 50 hours after the primary event. It was almost an order of magnitude increase in the low energy particles as seen in Figure 12. This was followed by a small recurring event (Figure 13) some 27 days later when the same solar region again passed central meridian.

It now appears that these recurring events are a common feature of active regions. However, they contain predominantly low energy particles, i.e., less than ~50 Mev with steeply falling energy spectra, and do not change the picture in terms of the radiation hazards to man in space.

Consistent with these observations are the studies by Guss[35] of the distribution in heliographic longitude of flares which produce energetic solar particles. Guss has found that flares from a single 10^{o} interval in heliographic longitude caused most of the large solar particle events over the last solar cycle. He has interpreted this to indicate the existence of a center for the formation of active regions which persisted for more than 73 rotations. Figure 14 shows the heliographic longitudes for flares which produced solar particle events between 1955 and 1962 during the last solar cycle. The series of flares between 80^{o} and 90^{o} produced the largest particle events of that cycle - the event of 23 February 1956 and the multiple events of July 1959, November 1960, and July 1961. The remainder of the events during the last solar cycle also fall into longitude bands, but not so sharply defined. Guss found that the events between 240^{o} and 280^{o}, with one exception, occurred between 20 January 1957 and 23 March 1958, indicating the existence of an active site which lasted for more than a year. The events between 210^{o} and 220^{o} are those of March through September 1960. The interval between 160^{o} and 190^{o} contained events which occurred between 9 August 1957 and 10 May 1959. The interval between 110^{o} and 140^{o} includes events from 6 June 1958 to 22 August 1958 and the two small events of 10 September and 28 September 1961. Finally, he observed a dearth of activity in the longitude interval between 280^{o} and 80^{o}. Thus, a single well-defined longitude region was responsible for most of the intense particle events of the last solar cycle. The fact that this region can be compressed into a 10^{o} band of longitude with a suitable choice of the period of solar radiation would indicate that this site rotated at constant rate as observed through the variable rotation of the photosphere.

Several excellent summaries on solar protons have appeared. These include a review of solar cosmic ray events by W. R. Webber in the AAS-NASA Symposium on the Physics of Solar Flares[26] and D. K. Bailey[37] in the Tenth report of the Inter Union Commission on Solar and Terrestrial Relationships.

Figure Captions

1. Reproduction of tracks of primary cosmic rays of Hydrogen - Iron in nuclear emulsions.
2. Integral energy spectra of primary nucleons.
3. Low energy differential energy spectra of primary cosmic ray protons in time interval close to solar maximum.
4. Time history of three integral energy regions from November 12, 1960 event.
5. Time history of three integral energy regions from November 15, 1960 event.
6. Integral proton spectra are shown as exponentials in rigidity at selected times for 6 different solar flares. Data points taken from counter ascents are shown as solid symbols; those taken with emulsion as open symbols.
7. Time history of the intensity and spectrum of solar particles during the events of November 1960. The values of J_o are determined by various techniques and includes riometer, balloon, rocket, satellite and neutron monitors.
8. The intensities of 87-Mev protons vs time after the type IV emissions during the five primary solar proton events. The shapes of only two events, those of 28 September 1961 and 23 October 1962, are seen to be quantitatively similar, as monitored in this manner.
9. The differential intensities of solar protons during the 28 September 1961 event plotted against time after the X-ray burst at the sun. The data

are interrupted when the satellite passed through the magnetosphere and when the delayed increase occurred on 30 September 1961.

10. The intensity vs time plots for the 28 September 1961 (Figure 9) converted to relative intensity vs distance plots. The distance is computed for each energy component by taking the product of the corresponding particle velocity and time from the event; the intensities are scaled to give the best fit to a common propagation curve. This fit occurs over a dynamic range in energy of a few hundred and a velocity range of 14, and over a time duration of several days.
11. The source spectra of three solar proton events. The intensities plotted are arbitrarily chosen to show the maximum intensities reached at the earth; as explained in the text the relative scaling of the two sections of the spectrum of 10 November is not necessarily meaningful. In the case of the solar proton events which totally conform to a velocity-dependent behavior, such as those of 28 September 1961 and 23 October 1962, the source spectrum is the unique differential energy spectrum of the protons at the time of their escape from the sun; in each event the source spectrum is proportional to that shown here with a constant which depends in an unknown way on the geometry of propagation.
12. Representative proton intensities between 28 September and 7 October, showing the delayed intensity increase of predominately lower-energy protons on 30 September 1961. The energy spectra of these particles are relatively constant with time, unlike those of the velocity-ordered primary solar proton event, and their arrival times are essentially constant with energy, occurring at the time of arrival of the enhanced solar plasma, two days after the flare.

13. The intensity of protons of energy above 3 Mev between 30 September and 28 October 1961. The delayed increase on 30 September is superposed on the primary solar-proton intensity decay and the recurrent event on 27 October follows the completely event-free intervening period.

14. Number of solar particle events vs heliographic longitude with the central meridian during the 23 February 1956 event set to 0°, and assuming a rotation period of 27.04 days. The particle intensity with kinetic energy > 30 Mev detected at the earth[8] integrated over the particle event is X , $I \geq 10^8$ particles/cm^2; 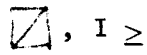 , $I \geq 5 \times 10^6$ particles/cm^2; open squares, $I < 5 \times 10^6$ particles/cm^2. A dot in a square signifies that there was a neutron-monitor rate increase, indicating the presence of a significant number of particles with kinetic energy greater than about 5000 Mev. Light lines are used to separate individual events and heavy lines to separate individual active regions.

References

1. A. D. Dainton, P. H. Fowler and D. W. Kent, Phil. Mag. 43, 729, 1952.

2. F. B. McDonald, NUOVO CIMENTO SUPPLEMENT 8, 500 (1958).

3. C. J. Waddington, J. Phys. Soc. Japan 17, Supplement A-3 63, 1962.

4. G. D. Badhwar, R. R. Daniel and B. Vijayalakshmi, Prog. Theor. Phys. 28, 607, 1962.

5. J. A. Earl, Phys. Rev. Ltrs. 6, 125, 1961.

6. P. Meyer and R. Vogt, Phys. Rev. Ltrs. 6, 193, 1961.

7. J. Linsley, Phys. Rev. Ltrs. 10, 146 (1963).

8. F. B. McDonald, Phys. Rev. 109, 1367, 1958.

9. W. R. Webber and F. B. McDonald, Journal of Geophysical Research, 69, 3097, 1964.

10. G. Brooke, P. J. Hayman, Y. Kamiya and A. W. Wolfendale, Nature 198, 1293 (1963).

11. L. T. Baradzei, V. I. Rubtsov, Y. A. Smorodin, M. V. Solouyov and B. V. Tolkachew, J. Phys. Soc. Japan 17, Supplement A-III, 433 (1962).

12. J. Delvaille, F. Kenoziorski and K. Greisen, J. Phys. Soc. Japan, 17, Supplement A-III, 76, 1962.

13. J. Linsley, L. Scarsi and B. Rossi, J. Phys. Soc. Japan 17, Supplement A-III, 91, 1962.

14. S.N. Vernov, G.B. Khristiansen, V.I. Atrashkevich, V.A. Dimitriev, Yu. Fomin, B.A. Khrenov, G.V. Kulikov, Yu. A. Nuchin and V.A. Solviyeva, J. Phys. Soc. Japan 17, Suppl. AIII, 118 (1962).

15. F. B. McDonald and G. H. Ludwig, To be published in Phys. Rev. Letter, 1964.

16. V. K. Balasubrahmanyan and F. B. McDonald, Journal of Geophysical Research 69, 3289, 1964.

17. C. E. Fichtel, D. E. Guss, D. A. Kniffen and K. A. Neelakantan, Journal of Geophysical Research 69, 3293, 1964.

18. P. S. Freier and C. J. Waddington, Physical Review Letters 13, 108 (1964).

19. J. Ormes and W. R. Webber, Physical Review Letters 13, 106 (1964).

20. A. M. Conforto, J. Phys. Soc. Japan 17, Supplement A-III, 144, 1962.

21. K. Greisen, Progress in Cosmic Ray Physics, III, 1 (1956).

22. S. E. Forbush, Phys. Rev. 70, 771, 1946.

23. D. K. Bailey, Journal of Geophysical Research, 62, 431, 1957.

24. G. Reid and C. Collins, J. Atmospheric and Terrest. Phys. 14, 63, 1959.

25. H. Malitson and W. Webber, Solar Proton Manual, Goddard Space Flight Center, Publication # X-611-62-122, P1, 1962.

26. C. E. Fichtel, D. E. Guss and K. W. Ogilvie, Solar Proton Manual, Goddard Space Flight Center, Publication # X-611-62-122, P. 19, 1962.

27. K. G. McCracken, Journal of Geophysical Research, 67, 447, 1962.

28. S. Biswas and C. Fichtel, Astrophysical Journal 139, 941, 1964.

29. S. Biswas, C. E. Fichtel and D. E. Guss, Phys. Rev. 128, 2756, 1962.

30. P. S. Freier and W. R. Webber, Journal of Geophysical Research, 68, 1605, 1962.

31. Bryant, D.A., T. L. Cline and F.B.McDonald, NASA Tech.Publ. X611-64-217 "Studies of Solar Protons with Explorers XII and XIV". (To be published in Astrophysical Journal).

32. Bryant, D.A., T.L.Cline, U.D.Desai and F.B.McDonald, JGR 67, 4983, 1962.

33. E. N. Parker, "Interplanetary Dynamical Processes", Interscience, 1963, p. 210.

34. Huffman, D. J. and J. R. Winckler, JGR 68, 2067, 1963.

35. Guss, D. E., Phys.Rev.Letters 13, 363, 1964.

36. W. R. Webber, AAS-NASA Symposium on the Physics of Solar Flares, Ed. by W.Hess. NASA SP50 (1964).

37. D.K.Bailey, Planetary Space Science 12, 495, 1964.

TABLE I

CHEMICAL COMPOSITION

GALACTIC COSMIC RAYS

GROUP	Z	INTENSITY/ METER^2-STER-SEC $>$ 1.5 BEV/NUC	INTENSITY INTENSITY Z $\geq$ 10	AVERAGE IN UNIVERSE *
HYDROGEN	1	1300	680	3360
HELIUM	2	88	46	258
Li, Be, B	3 - 5	1.9	1.0	10^{-5}
C, N, O, F	6 - 9	5.7	3.0	2.64
Z $\geq$ NEON	$\geq$ 10	1.9	1.0	1
Z $\geq$ CALCIUM	$\geq$ 20	.53	0.28	.06

* AFTER SUESS AND UREY

TABLE 2

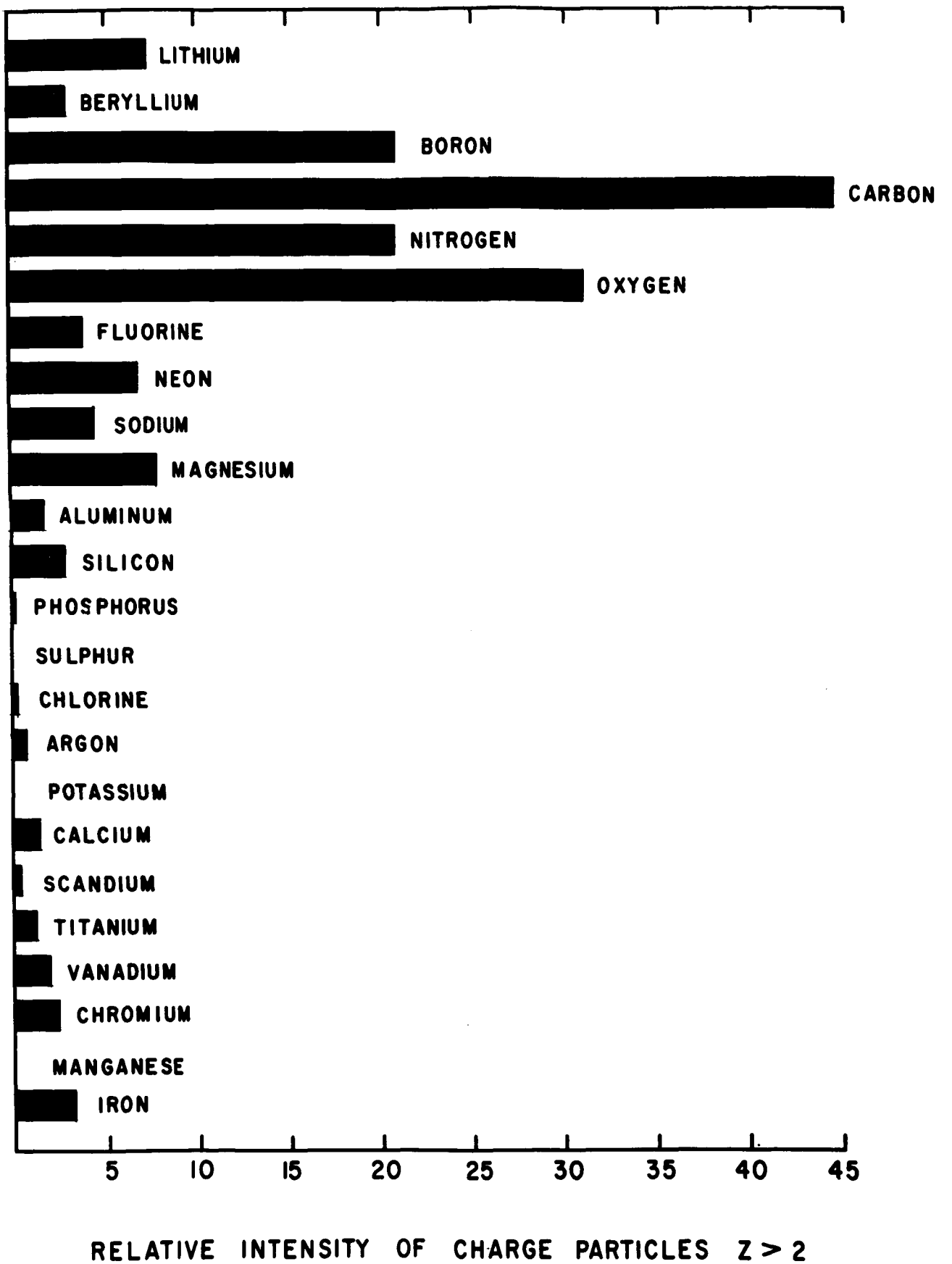
LITHIUM
BERYLLIUM
BORON
CARBON
NITROGEN
OXYGEN
FLUORINE
NEON
SODIUM
MAGNESIUM
ALUMINUM
SILICON
PHOSPHORUS
SULPHUR
CHLORINE
ARGON
POTASSIUM
CALCIUM
SCANDIUM
TITANIUM
VANADIUM
CHROMIUM
MANGANESE
IRON
5
10
15
20
25
30
35
40
45
RELATIVE INTENSITY OF CHARGE PARTICLES Z > 2

TABLE 3

YEAR	NO. OF SOLAR COSMIC RAY EVENTS	SOLAR COSMIC RAYS INTEGRATED INTENSITY PART/cm²/YEAR 30 MEV
1949	6	—
1950	4	—
1951	4	—
1952	0	—
1953	2	—
1954	0	—
1955	1	—
1956	5	8×10^9
1957	15	4×10^8
1958	12	1×10^9
1959	7	7×10^9
1960	12	5×10^9
1961	9	3×10^9
1962	2	—

TABLE 4

INTEGRATED INTENSITY-PART/CM^2	NO. OF EVENTS
$10^6 - 10^7$	8
$10^7 - 10^8$	10
$10^8 - 10^9$	5
$10^9 - 10^{10}$	6

TABLE V

RELATIVE ABUNDANCES OF NUCLEI NORMALIZED TO A BASE OF 1.0 FOR OXYGEN

Element	Solar Cosmic Rays	Sun	Universal Abundances	Galactic Cosmic Rays
$_2$He.....	107±14	?	150	48
$_3$Li.....	.....	<<0.001	<< 0.001	0.3
$_4$B-$_5$B.....	<0.02	<<0.001	<< 0.001	0.8
$_6$C.....	0.59 ±0.07	0.6	0.3	1.8
$_7$N.....	0.19 ±0.04	0.1	0.2	≤ 0.8
$_8$O.....	1.0	1.0	1.0	1.0
$_9$F.....	<0.03	<<0.001	<< 0.001	≤ 0.1
$_{10}$Ne.....	0.13 ±0.02	?	0.40	0.30
$_{11}$Na.....	.....	0.002	0.001	0.19
$_{12}$Mg.....	0.043±0.011	0.027	0.042	0.32
$_{13}$Al.....	.....	0.002	0.002	0.06
$_{14}$Si.....	0.033±0.011	0.035	0.046	0.12
$_{15}$P-$_{21}$Sc....	0.057±0.017	0.032	0.027	0.13
$_{22}$Ti-$_{28}$Ni	≤0.02	0.006	0.030	0.28

FIGURE I

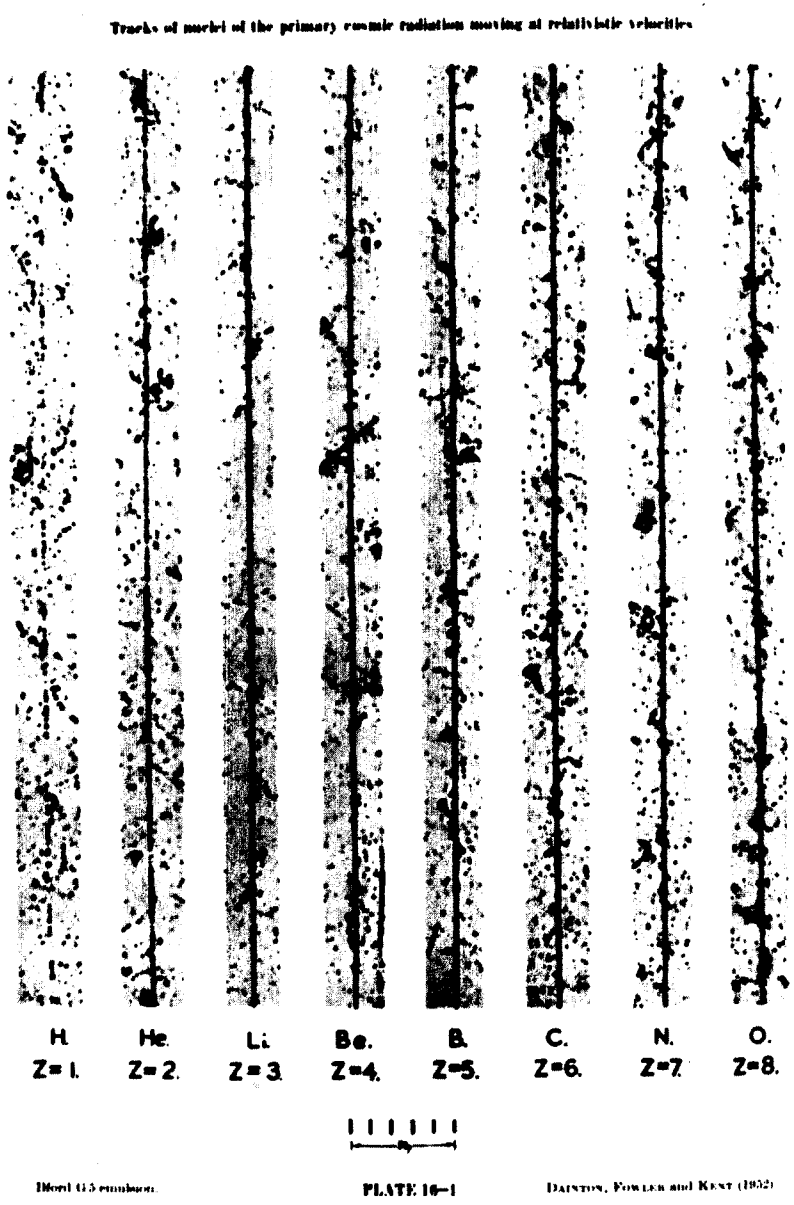

Ilford G5 emulsion. PLATE 16–1 DAINTON, FOWLER and KENT (1952)

The tracks were identified by measurements of scattering and δ-ray density.

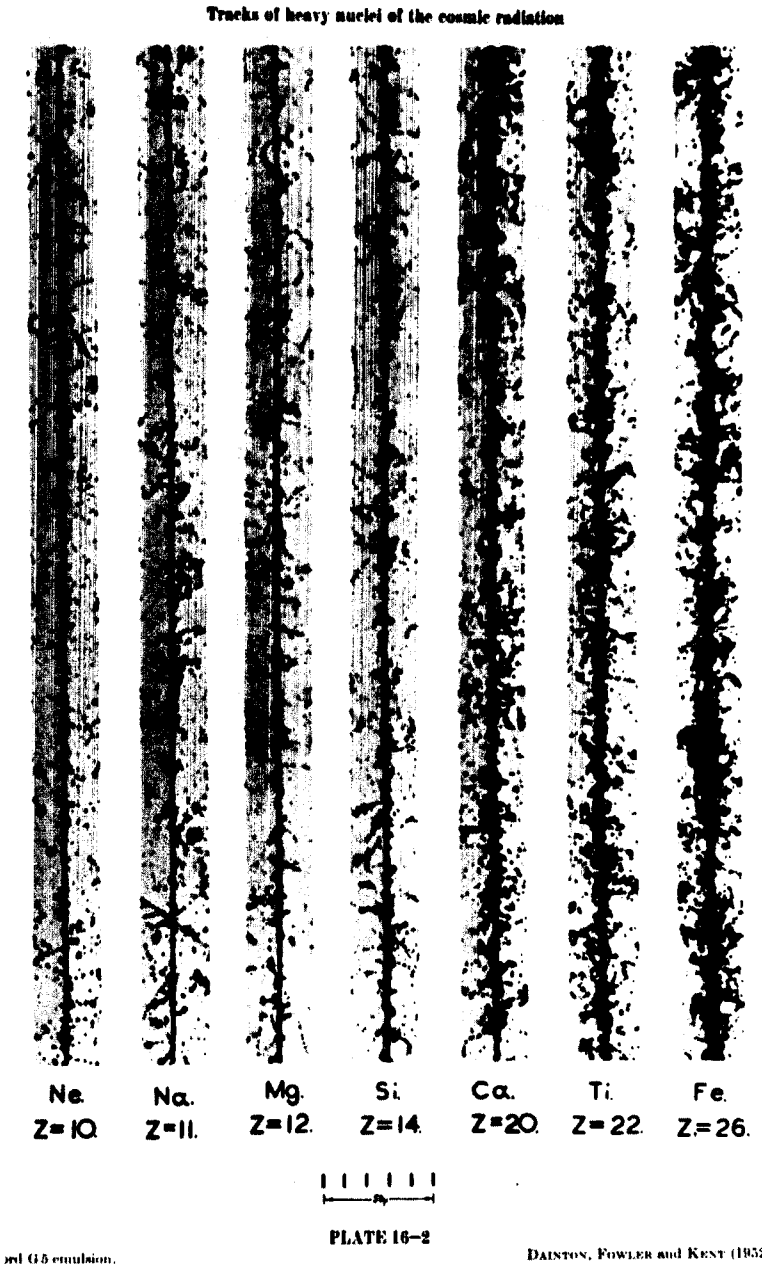

PLATE 16–2

ord G5 emulsion. DAINTON, FOWLER and KENT (1952).

The tracks were identified by measurements of scattering ($\bar{x}$), and δ-ray density (N_δ).

FIGURE 2

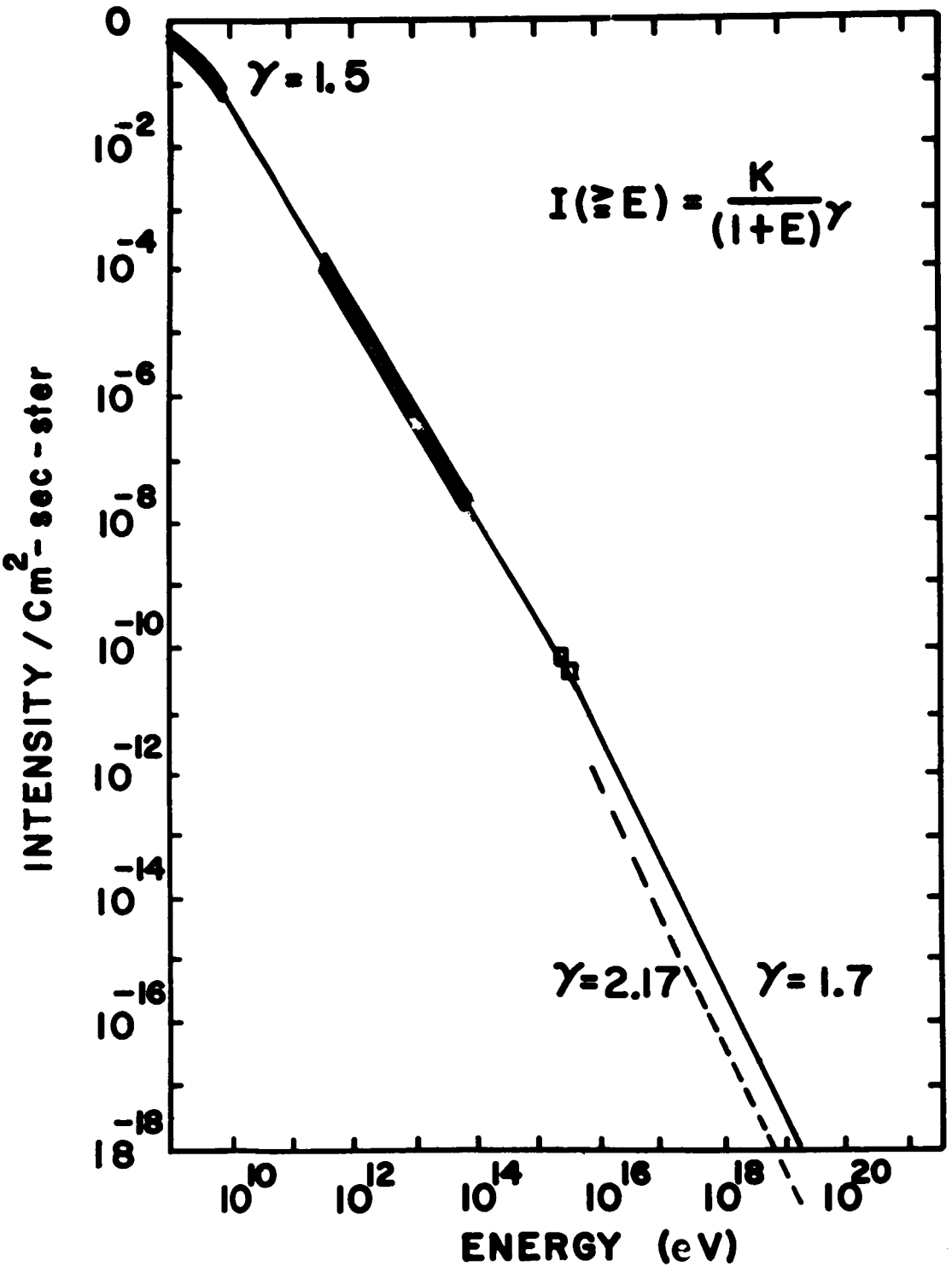

INTEGRAL ENERGY SPECTRUM OF PRIMARY NUCLEONS

FIGURE 3

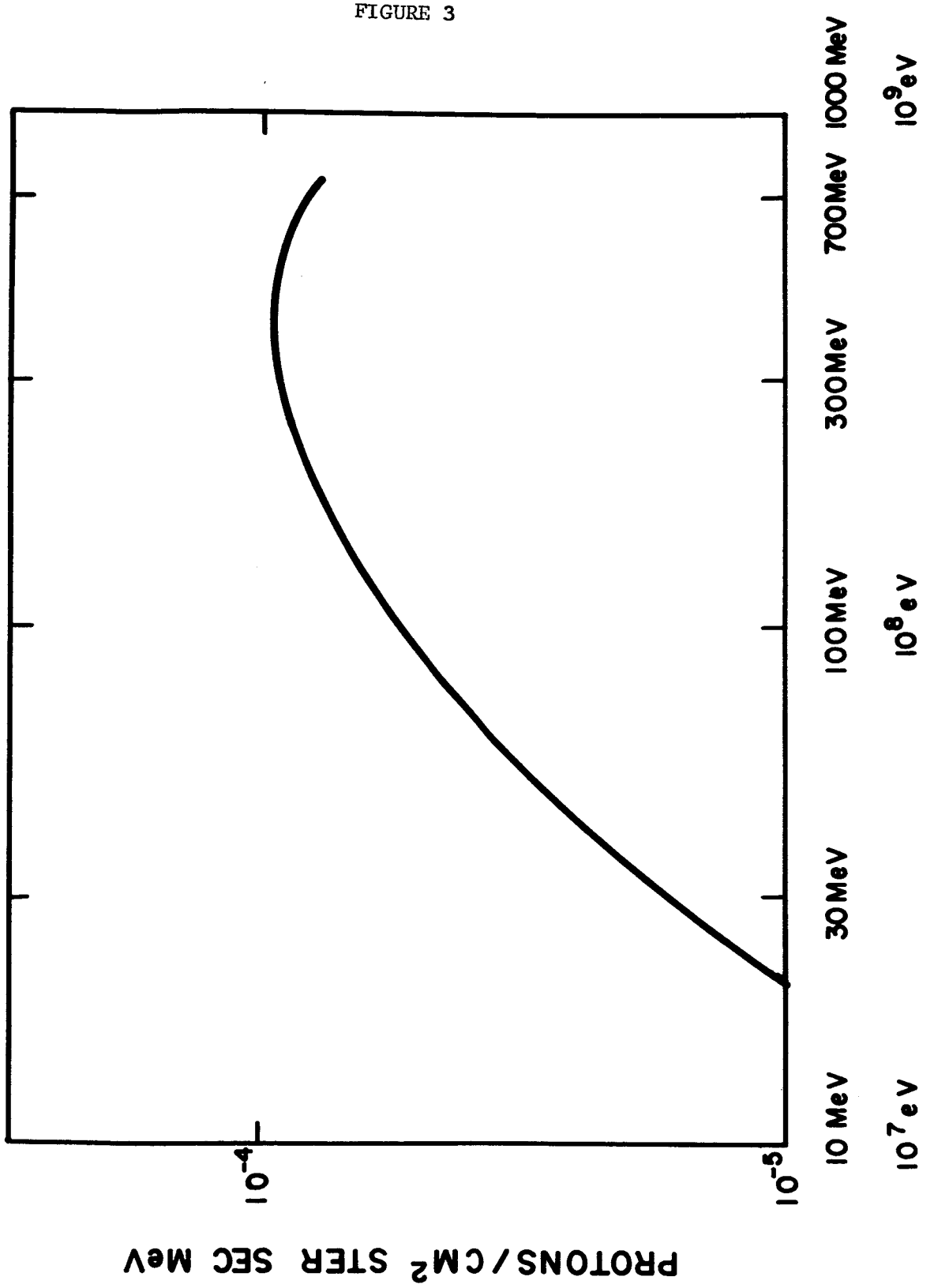
PROTONS/CM² STER SEC MeV
10⁻⁴
10⁻⁵
10 MeV
10⁷eV
30MeV
100MeV
10⁸eV
300MeV
700MeV
1000 MeV
10⁹eV
PROTON KINETIC ENERGY

FIGURE 4

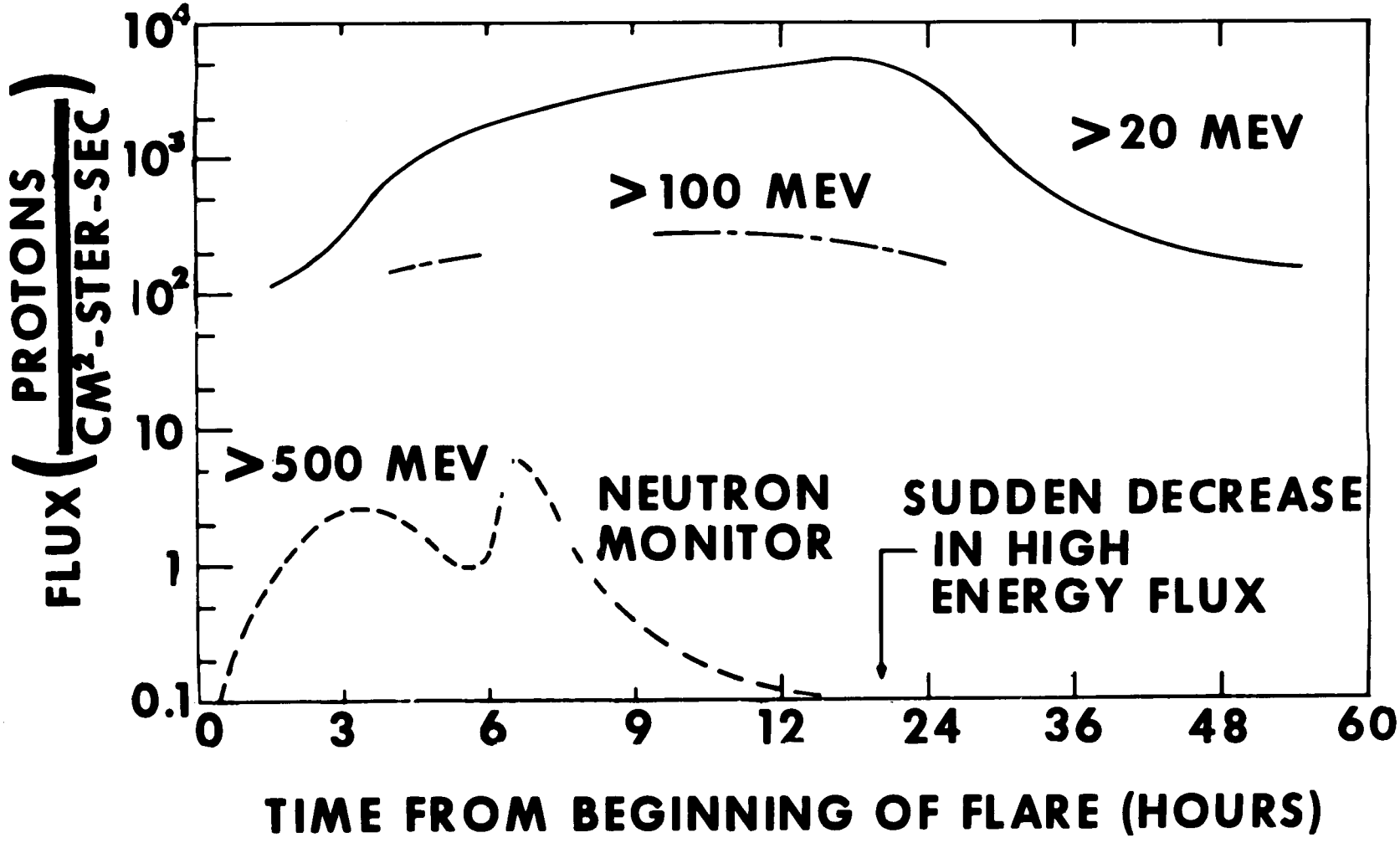
FLUX (PROTONS / CM²-STER-SEC)
10⁴
10³
10²
10
1
0.1
>20 MEV
>100 MEV
>500 MEV
NEUTRON MONITOR
SUDDEN DECREASE IN HIGH ENERGY FLUX
0
3
6
9
12
24
36
48
60
TIME FROM BEGINNING OF FLARE (HOURS)

FIGURE 5

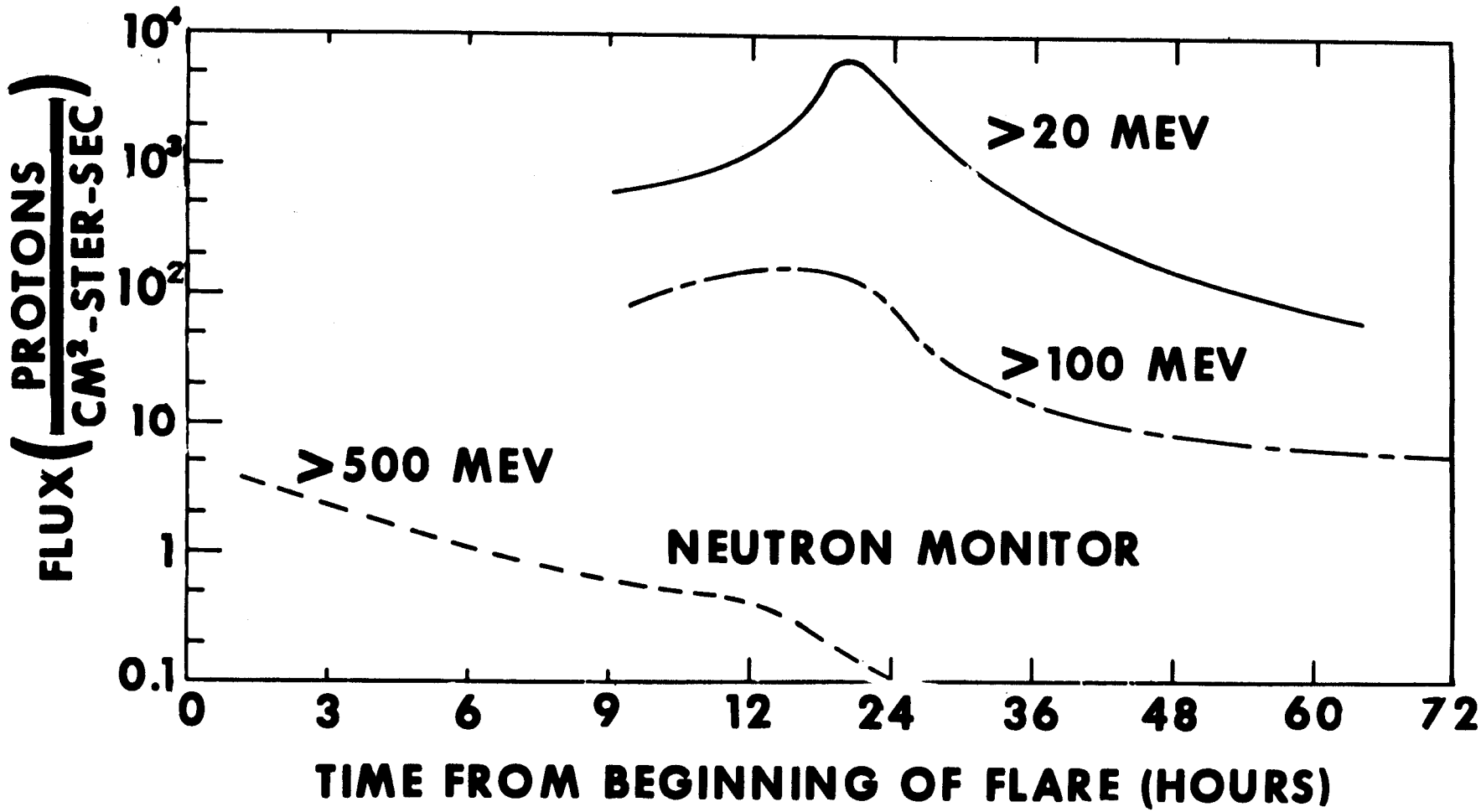
FLUX (PROTONS / CM²-STER-SEC)
10⁴
10³
10²
10
1
0.1
>20 MEV
>100 MEV
>500 MEV
NEUTRON MONITOR
0
3
6
9
12
24
36
48
60
72
TIME FROM BEGINNING OF FLARE (HOURS)

FIGURE 6

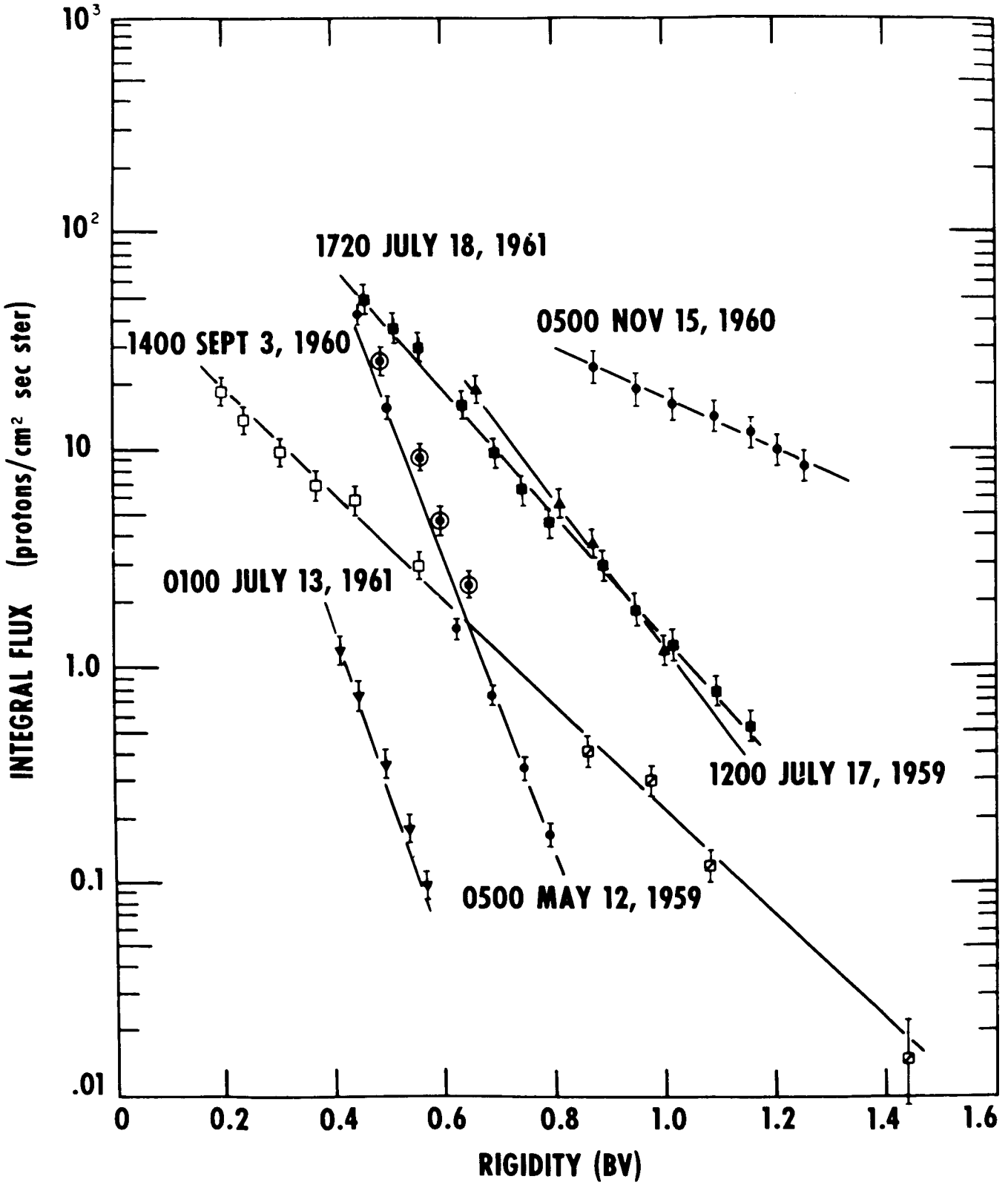
INTEGRAL FLUX (protons/cm² sec ster)
RIGIDITY (BV)
1720 JULY 18, 1961
0500 NOV 15, 1960
1400 SEPT 3, 1960
0100 JULY 13, 1961
1200 JULY 17, 1959
0500 MAY 12, 1959

FIGURE 7

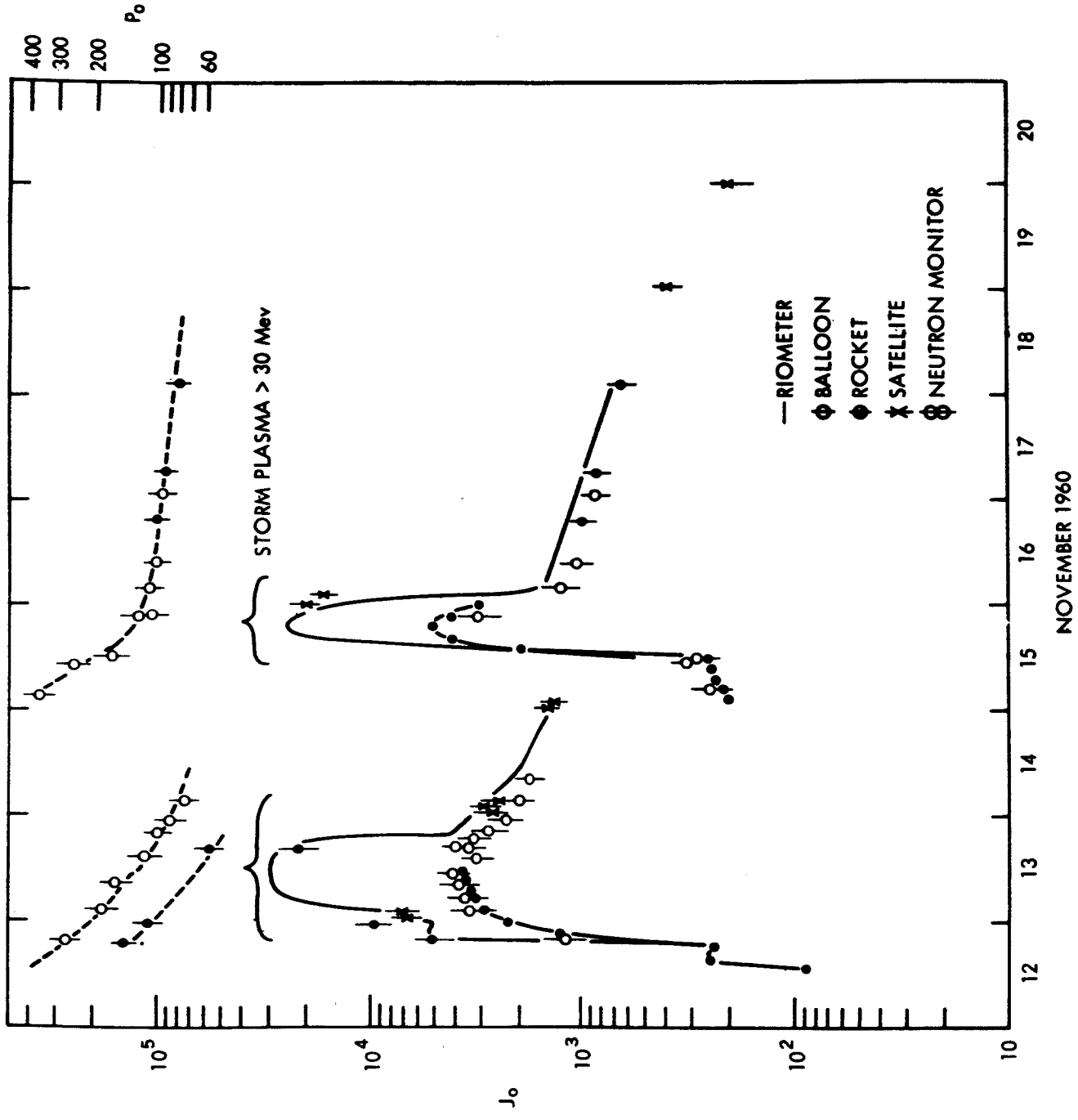
P_o
400
300
200
100
60
STORM PLASMA > 30 Mev
RIOMETER
BALLOON
ROCKET
SATELLITE
NEUTRON MONITOR
J_o
10^5
10^4
10^3
10^2
10
12
13
14
15
16
17
18
19
20
NOVEMBER 1960

FIGURE 8

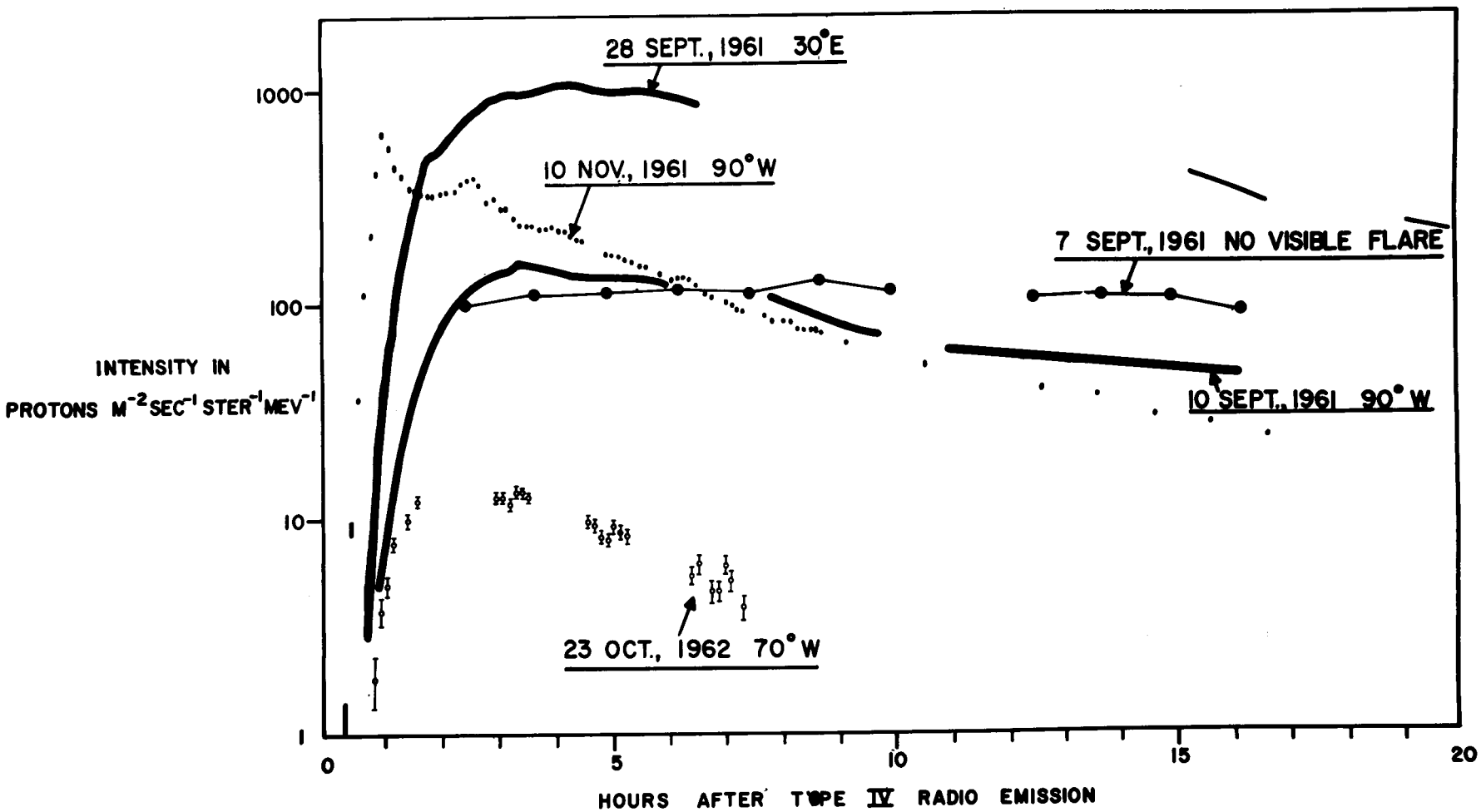

INTENSITY OF 85 MEV PROTONS
DURING FIVE SOLAR PROTON EVENTS

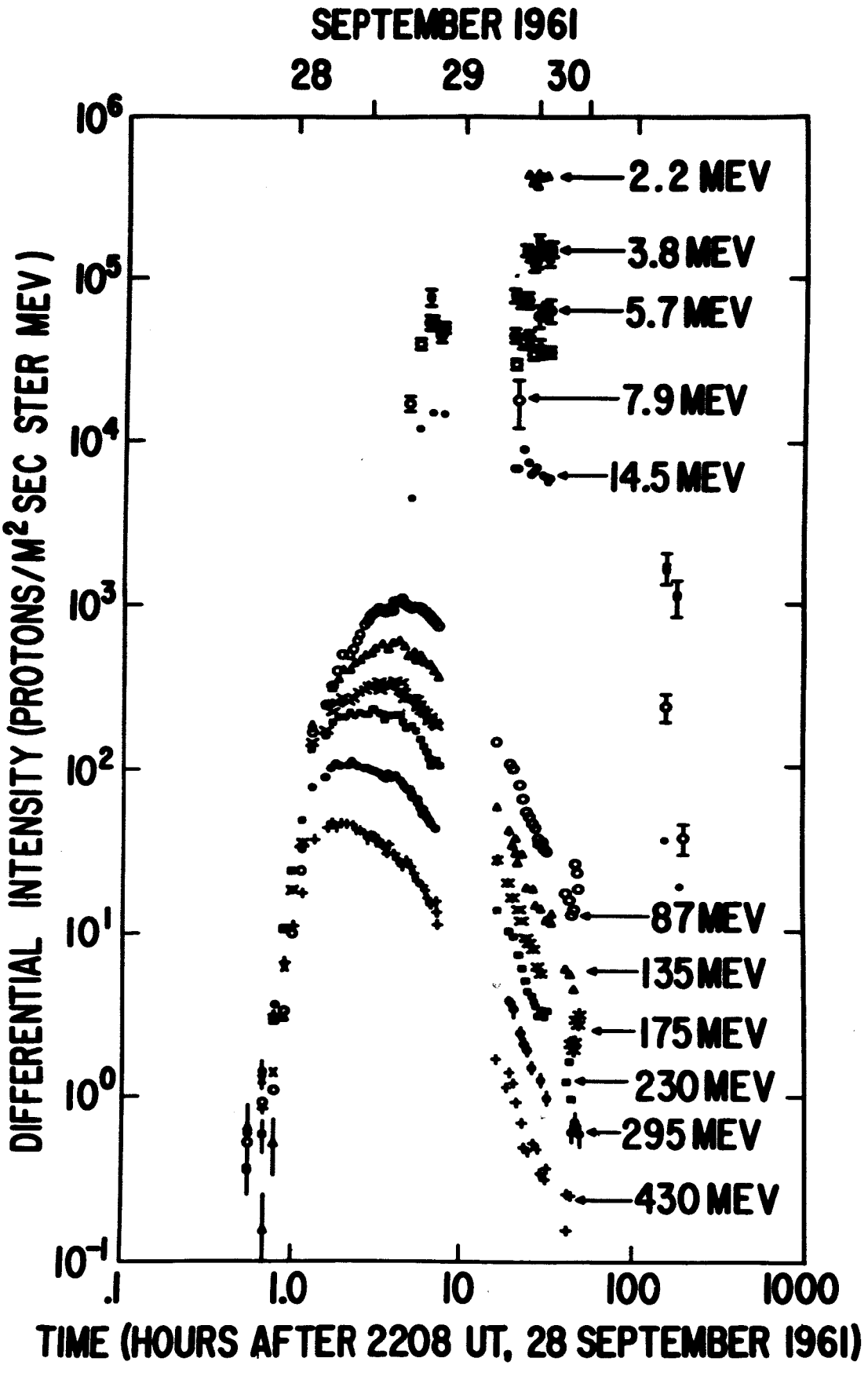
SEPTEMBER 1961
28
29
30
10^6
10^5
10^4
10^3
10^2
10^1
10^0
10^{-1}
DIFFERENTIAL INTENSITY (PROTONS/M² SEC STER MEV)
2.2 MEV
3.8 MEV
5.7 MEV
7.9 MEV
14.5 MEV
87 MEV
135 MEV
175 MEV
230 MEV
295 MEV
430 MEV
.1
1.0
10
100
1000
TIME (HOURS AFTER 2208 UT, 28 SEPTEMBER 1961)

FIGURE 9

FIGURE 10

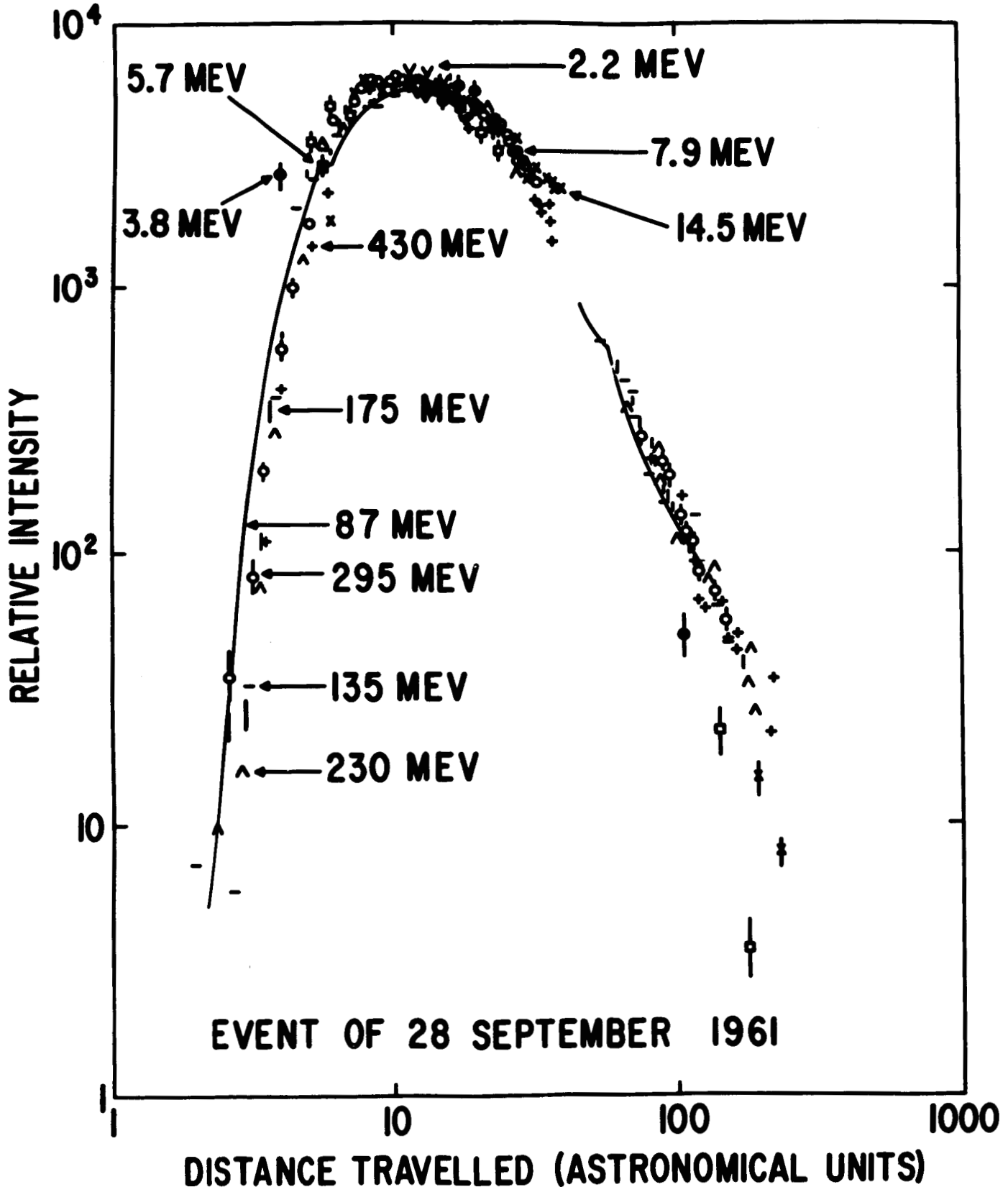
10⁴
10³
10²
10
1
RELATIVE INTENSITY
5.7 MEV
2.2 MEV
7.9 MEV
3.8 MEV
430 MEV
14.5 MEV
175 MEV
87 MEV
295 MEV
135 MEV
230 MEV
EVENT OF 28 SEPTEMBER 1961
1
10
100
1000
DISTANCE TRAVELLED (ASTRONOMICAL UNITS)

FIGURE 11

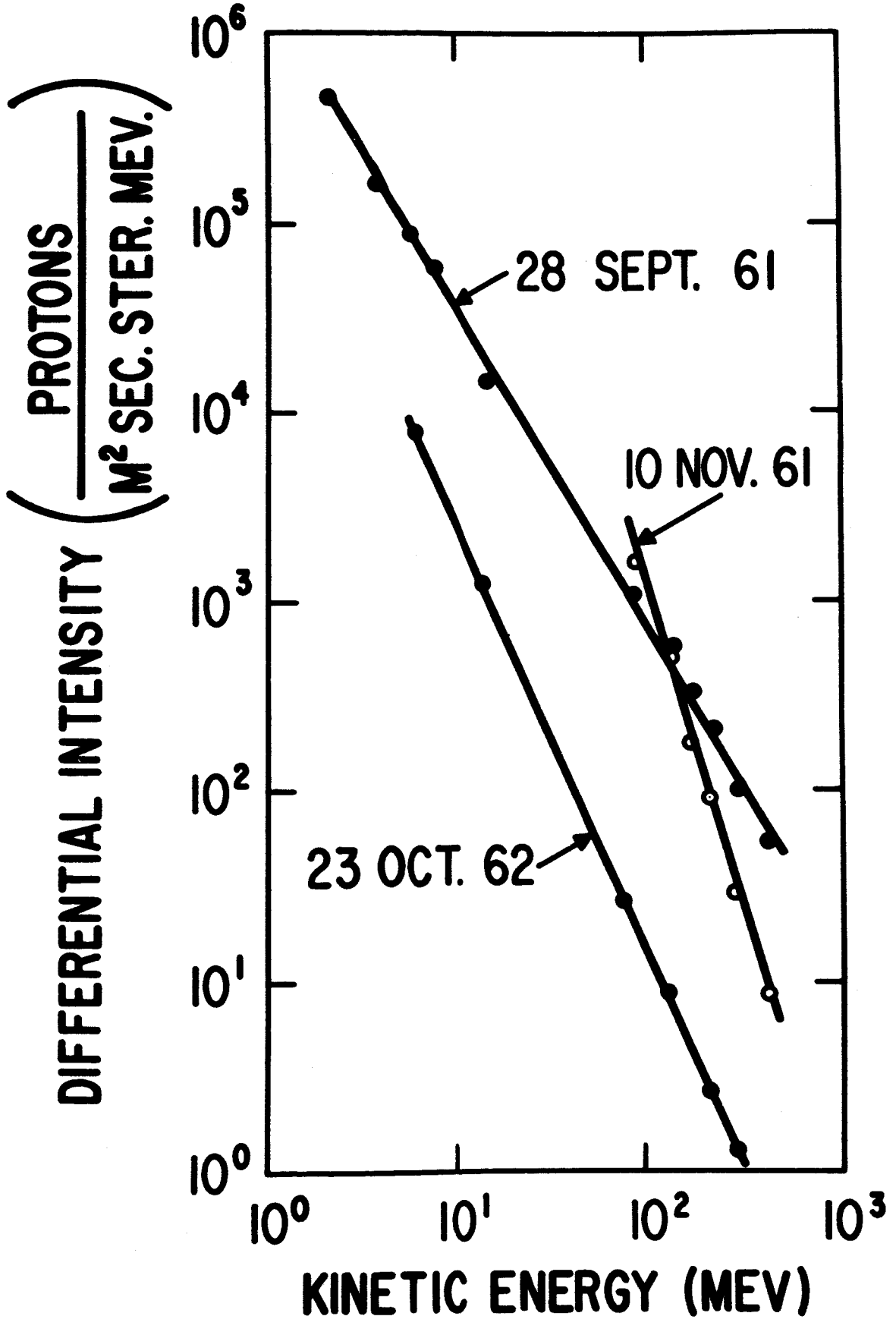
DIFFERENTIAL INTENSITY (PROTONS / M² SEC. STER. MEV.)
10⁶
10⁵
10⁴
10³
10²
10¹
10⁰
28 SEPT. 61
10 NOV. 61
23 OCT. 62
10⁰
10¹
10²
10³
KINETIC ENERGY (MEV)

FIGURE 12

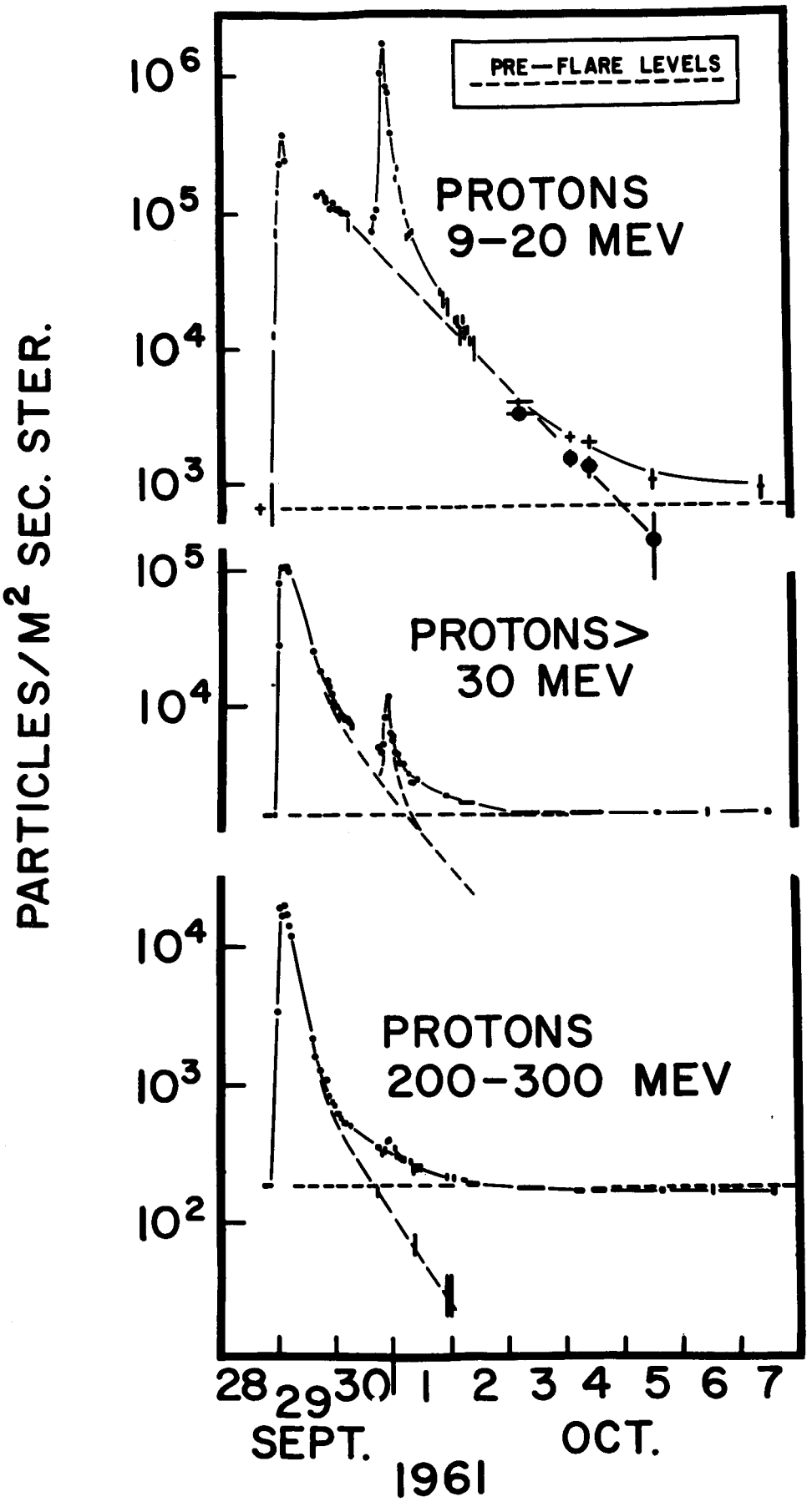
PRE—FLARE LEVELS
PROTONS
9–20 MEV
PROTONS>
30 MEV
PROTONS
200–300 MEV
PARTICLES/M² SEC. STER.
10⁶
10⁵
10⁴
10³
10⁵
10⁴
10⁴
10³
10²
28 29 30 1 2 3 4 5 6 7
SEPT.
OCT.
1961

FIGURE 13

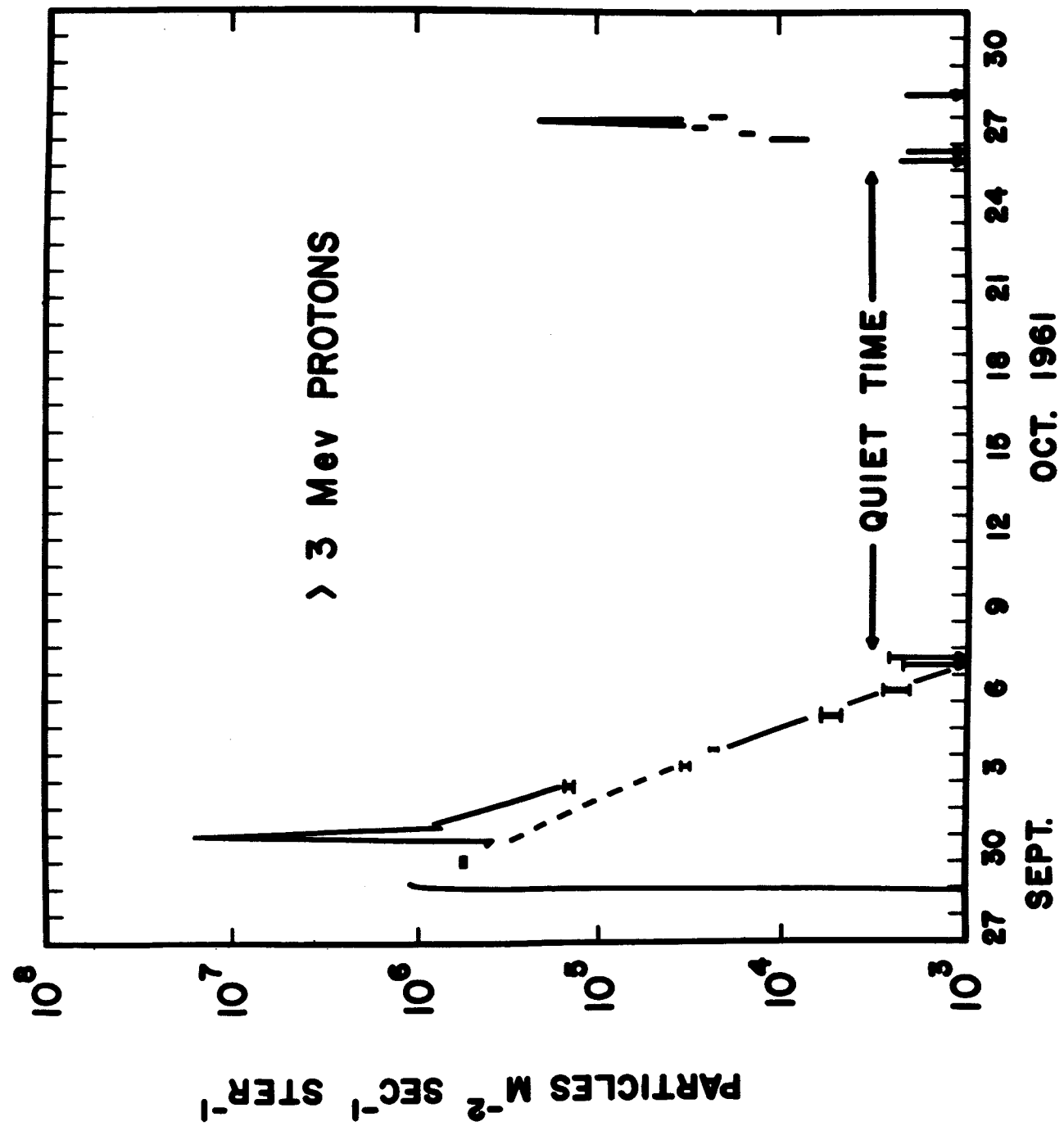
> 3 Mev PROTONS
QUIET TIME
PARTICLES M^{-2} SEC^{-1} STER^{-1}
10^8
10^7
10^6
10^5
10^4
10^3
SEPT.
27
30
3
6
9
12
15
18
21
24
27
30
OCT. 1961

FIGURE 14

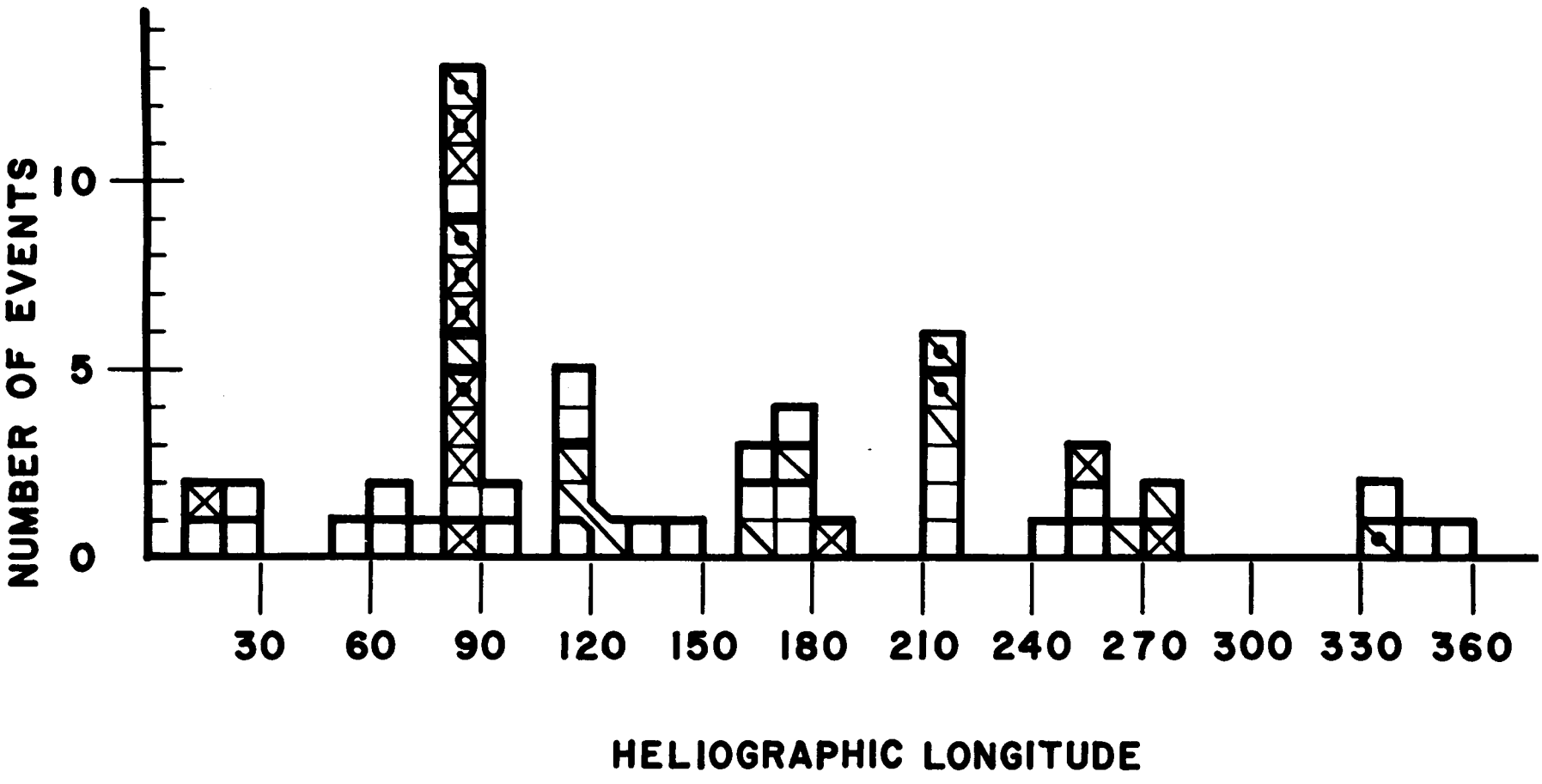
NUMBER OF EVENTS
0
5
10
30
60
90
120
150
180
210
240
270
300
330
360
HELIOGRAPHIC LONGITUDE